Thermal decomposition of the HXeCl···H_2O complex in solid xenon: Experimental characterization of the two-body decomposition channel

Masashi Tsuge,[a,b,*] Markku Räsänen,[b] and Leonid Khriachtchev[b]

[a] *Institute of Low Temperature Science, Hokkaido University, Sapporo 060-0819, Japan*

[b] *Department of Chemistry, University of Helsinki, P.O. Box 55, FIN-00014, Finland*

[*]Corresponding Author:

Postal address: Kita-19, Nishi-8, Kita-ku, Sapporo 060-0819, Japan

E-mail: tsuge@lowtem.hokudai.ac.jp

Tel: +81(11)706-5474

Keywords: noble-gas hydride, molecular complex, infrared spectroscopy, matrix-isolation

HIGHLIGHTS

- The $HXeCl\cdots H_2O$ complex is thermally decomposed in solid Xe above 42 K.
- Thermal decomposition product from HNgY molecules is identified for the first time.
- The decomposition path is experimentally characterized as two-body decomposition.
- Quantum-chemical calculations qualitatively reproduce the experimental results.

GRAPHICAL ABSTRACT

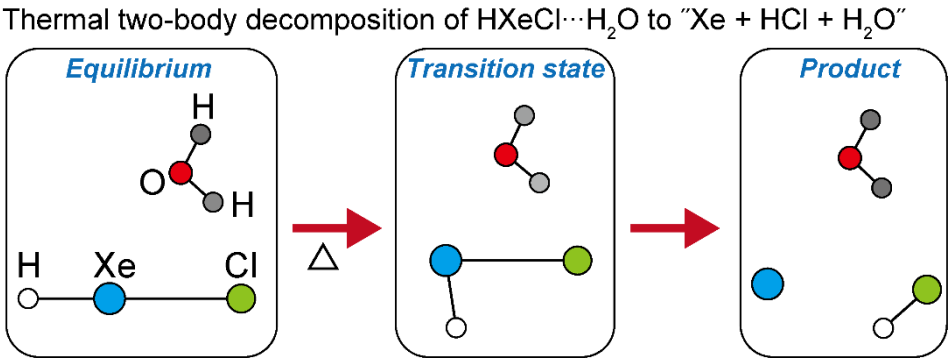

ABSTRACT

The thermal decomposition process of $HXeCl\cdots H_2O$ in solid Xe is studied, and $HCl\cdots H_2O$ is identified as a decomposition product. The production is due to the two-body (2B) decomposition of HXeCl moiety, in agreement with theoretical predictions. Two types of 2B decomposition paths are predicted: catalytic and unimolecular 2B decompositions, where water molecule plays different roles. In an experiment to selectively produce $HXeCl\cdots D_2O$, only $HCl\cdots D_2O$ is observed as a thermal decomposition product, indicating the occurrence of unimolecular 2B decomposition, where water molecule serves as a spectator. The activation energy for this decomposition process is experimentally determined to be 15 kJ mol^{-1}.

1. Introduction

Noble-gas hydrides with the general formula HNgY, where Ng = noble gas atom and Y = electronegative fragment, have been extensively studied both experimentally and theoretically after the first identification by Pettersson et al. in 1995 [1-3]. About 30 species, including the first neutral argon compound HArF [4], have been experimentally identified mostly in noble-gas matrices with the latest members of HKrCCCl, HXeCCCl, and C_6H_5CCXeH [5,6]. The HNgY molecules are produced typically by the following procedure; photolysis of HY in solid Ng produces H and Y fragments and the subsequent annealing of the matrix mobilize H atom, leading to the formation of HNgY. The bonding motif of HNgY molecules is represented in the form $(H–Ng)^+Y^–$, where the $(H–Ng)^+$ part is mainly covalent and the interaction between $(HNg)^+$ and $Y^–$ groups is predominantly ionic [7,8].

As compared to extensive studies on the spectroscopy of HNgY, especially in the infrared (IR) region probing very intense H–Ng stretching modes, the number of studies addressing the kinetic stability of HNgY is quite small. A typical energy diagram of HNgY species is shown in Fig. 1. The equilibrium structure of HNgY is metastable with respect to the ″HY + Ng″ asymptote and lower in energy than the ″H + Ng + Y″ asymptote. Note that HNgY molecules can be produced in experiments only when the H + Ng + Y → HNgY process is exothermic [9]. Regardless of this fact, there are many predictions on new HNgY species whose association process is endothermic; i.e., it is probably impossible to produce these predicted species by experiment.

Two thermal decomposition channels of HNgY have been discussed [2,10]:

$$HNgY \rightarrow HY + Ng, \quad (1)$$

$$HNgY \rightarrow H + Ng + Y. \quad (2)$$

The first reaction, often referred to as the two-body (2B) decomposition channel, is always highly exoergic but the bending barrier is sufficiently high to ensure the stability of HNgY species at low temperatures (~ 10 K). The second reaction is referred to as the three-body (3B) decomposition channel, which occurs along the stretching coordinate. It has been reported that some of HNgY molecules decompose in matrices at elevated temperatures. The first indication of thermal decomposition of HNgY molecules was reported in 1996: the decay of HXeH at 75–80 K [11]. Later, HXeOH was found to decompose in a Xe matrix at 54 K and HXeBr at 60 K [12,13]. It is generally considered that the thermal stability of HNgY molecules is mainly controlled by the 3B decomposition channel [2]; i.e., 3B-TS is lower in energy than 2B-TS as shown in Fig. 1. We found that the thermal decomposition rate of HXeBr in a carbon dioxide (CO_2) ice is much slower than that in a Xe matrix [13]. The significant blue shift of the H–Xe stretching mode of HXeBr from 1504 cm^{-1} in Xe to 1646 cm^{-1} in CO_2 indicates the stabilization with respect to the 3B decomposition channel and, therefore, this observation might be consistent with theoretical predictions that the stability is controlled by the 3B decomposition channel.

However, the energetic stabilization or destabilization of HNgY molecule by a matrix is still unclear; there are a few experimental studies on the environmental effects on HNgY molecules [14-16]. Khriachtchev et al. studied relative stabilities of HXeOH and HXeOXeH in a Xe matrix at 55 K and found that HXeOXeH is more stable than HXeOH [17]. This experimental result is in complete disagreement with the theoretical predictions [18]. The discrepancy might originate from the fact that theoretical calculations are done for species in vacuum whereas the experiments are done for the species in the solid phase. There are some attempts to model the environmental effect on HNgY; e.g., on the H–Ng

stretching frequencies of HNgY in different matrices [15,19-23]. Among these studies, the methodology developed by Nakayama and co-workers could reproduce the experimentally observed order of H–Ng stretching frequencies [15,19].

Formation of molecular complex can also affect the thermal stability of HNgY molecules. The experimentally observed HNgY complexes are generally characterized by blue shifts of the H–Ng stretching mode [24]. For example, a very large blue shift ~300 cm^{-1} was reported for the HKrCl···HCl complex [25], which might be the largest blue shift among the reported neutral 1:1 complexes. The blue shift is considered as the ″normal effect″ for complexes of HNgY and has been explained by the enhancement in ion-pair character, $(HNg)^{+}Y^{-}$, upon complexation. More specifically, charge transfer from the antibonding orbital of H–Ng bond to the Y fragment is enhanced upon complexation, resulting in a shortening of the H–Ng bond and a blue shift of the H–Ng stretching frequency [2,24-27]. We have investigated the degree of spectral shifts in the HXeY···HX complexes (X, Y = Cl, Br, and I) and HXeY···H_2O complexes (Y = Cl, Br, and I) [28-30], and found that the shift is smaller for more strongly bound molecules. The enhancement in the ion-pair character not only affect the H–Ng stretching frequency but also the 2B decomposition barrier; the 2B decomposition barrier becomes smaller when the ion-pair character is enhanced. Therefore, one can expect that the 2B decomposition barriers in HNgY complexes are smaller than corresponding HNgY monomers and the 2B and 3B decomposition channels might compete in the thermal decomposition of HNgY complexes.

In this work, we investigated the thermal stability of the HXeCl···H_2O complex in a Xe matrix and found that this complex is less stable than the HXeCl monomer. The identification of thermal decomposition product from the HXeCl···H_2O complex allowed

us to characterize the decomposition channel to be 2B decomposition. From the temperature dependence of thermal decomposition rate, we determined the activation energy for the 2B decomposition of the HXeCl···H_2O complex.

2. Computational details and results

Quantum chemical calculations were performed by using the MOLPRO (Version 2010.1), GAUSSIAN 09 (Revision D.01), and GAUSSIAN 16 (Revision B.01) programs. The geometry optimizations, calculations of relative energies, and harmonic vibrational analyses were performed by the CCSD(T) and MP2(full) methods. The def2-TZVPPD basis sets for H, Cl, and Xe atoms, which are triple-zeta-valence basis sets augmented with two sets of polarization and diffuse basis functions, are obtained from the EMSL Basis Set Library [31]. For Xe atom, 28 electrons are replaced by an effective core potential. The basis set superposition error (BSSE) is corrected using the counterpoise procedure [32]. Zero-point vibrational energies were calculated using harmonic frequencies without scaling factors.

Figure 2 shows the structures of the HXeCl···H_2O complex at the equilibrium and transition states (TSs) for the 2B decomposition reaction optimized with the CCSD(T)/def2-TZVPPD method. Two transition states, catalytic and unimolecular TSs, were found. In the catalytic 2B-TS, the H atom in the HXeCl moiety is bent toward the H_2O moiety. In the unimolecular 2B-TS, on the other hand, the H atom is bent toward the opposite direction. At both TS, the H–Xe bond length is shortened and the Xe–Cl bond length is lengthened with respect to those in the equilibrium structure.

The intrinsic reaction coordinate calculations were performed for these TSs with the MP2/def2-TZVPPD method and the results are presented in Fig. 3. As the catalytic 2B

decomposition progresses, the H atom in the HXeCl moiety is transferred to the H_2O moiety and the H atom of H_2O moiety adjacent to the Cl atom moves toward the Cl atom. As a result, one of the H atoms in the H_2O moiety is exchanged with the H atom originally in the HXeCl moiety. In the unimolecular 2B decomposition path, the H_2O moiety serves as a spectator and thus the H and Cl atoms in the HXeCl moiety produces the HCl product. It is of note that these two decomposition channels can be distinguished in experiments using isotopically labeled species; e.g., the HXeCl···D_2O complex decomposes to DCl + Xe + HDO through the catalytic 2B decomposition path and to HCl + Xe + D_2O through the unimolecular 2B decomposition path.

The calculated 2B decomposition barriers and 3B dissociation energies of the HXeCl monomer and the HXeCl···H_2O complex are listed in Table 1. Calculations were performed with the MP2(full) and CCSD(T) methods. The Xe matrix environment was modeled by using the polarizable continuum model (PCM) [33]. Because PCM is not available for the CCSD(T) method, the matrix effect was taken into account for the CCSD(T) calculations using the MP2 correction: i.e., $E_{\mathrm{CCSD(T)+PCM}} = E_{\mathrm{CCSD(T)}} \times \frac{E_{\mathrm{MP2+PCM}}}{E_{\mathrm{MP2}}}$. The Xe matrix environment seems to significantly reduce the 2B barrier height. For the HXeCl monomer, $E_{\mathrm{CCSD(T)}}$ = 131 kJ mol^{-1} calculated for isolated species is reduced to $E_{\mathrm{CCSD(T)+PCM}}$ = 97 kJ mol^{-1}. The barrier heights for the catalytic and unimolecular 2B decomposition are the same within computational accuracy, ~62 kJ mol^{-1} after PCM correction to the CCSD(T) energy. The agreement is thought to be a coincidence and, if environmental effect could be accurately considered, the barrier heights of these two decomposition channels will be different (see Sec. 4). Calculation of the 3B decomposition *barrier* requires the multireference electron correlation methods [10,34,35]. Instead of barrier, the 3B *dissociation energies* were calculated as the energy

difference between 3B dissociation limit and the equilibrium structure. The 3B dissociation energy of the HXeCl monomer, 78 kJ mol^{-1}, calculated with the CCSD(T) method is slightly lower than the 3B decomposition barrier, 96 kJ mol^{-1}, calculated with the icMRCI+Q method [36]. We did not attempt to include the effect of Xe environment to the 3B dissociation energies. Because Xe environment is expected to stabilize HNgY molecules with respect to the stretching coordinate [15], the 3B dissociation energies in a Xe matrix would be higher than those calculated for species in vacuum. By forming the complex, the 2B dissociation barrier height becomes lower and the 3B dissociation energy becomes larger. As mentioned earlier, these changes can be rationalized by considering the enhancement of ion-pair character, $(HXe)^+Cl^-$, upon complexation. The calculated energies indicate that the thermal decomposition of HXeCl monomer occurs via the 3B channel whereas that of the $HXeCl\cdots H_2O$ complex occurs via the 2B channel.

Ionic dissociation channels were also examined. We assume that dissociated proton produces $XeHXe^+$ species with Xe atoms in HXeCl and in the vicinity, and Cl^- forms the $Cl^-\cdots H_2O$ complex. Therefore, this ionic dissociation channel is written as $Xe + HXeCl\cdots H_2O \rightarrow XeHXe^+ + Cl^-\cdots H_2O$. In addition, proton transfer reaction from HXeCl to H_2O, $HXeCl\cdots H_2O \rightarrow Xe + H_3O^+ + Cl^-$ was examined. The dissociation energies of these ionic dissociation channels are significantly higher (>400 kJ mol^{-1}) than neutral 2B dissociation barriers and the neutral 3B dissociation energies, suggesting that ionic channels do not contribute to the thermal decomposition of the $HXeCl\cdots H_2O$ complex.

3. Experimental details and results

The gaseous mixture of HCl (≥99.8%, Linde) and Xe (≥99.999%, AGA) with a mixing ratio HCl/Xe = 1/1000 was made in a glass flask by standard manometric

procedure. The second flask with a droplet of H_2O (or D_2O) was filled with Xe. The HCl/H_2O/Xe or HCl/D_2O/Xe matrices were deposited through two separate capillaries connected to each flask onto a CsI substrate kept at 40 K in a closed-cycle helium cryostat (RDK-408D2, SHI). The mixing ratio of water in the matrices was roughly estimated to be in the range 1/1000–1/2000. For the deposition of HCl/D_2O/Xe matrices, the deposition line for D_2O/Xe was heavily flushed with this mixture before the matrix deposition and the deposition line for the HCl/Xe mixture contained a droplet of H_2SO_4 to remove H_2O impurity. As a result, the HCl/D_2O/Xe matrices with practically no H_2O and HDO were successfully obtained. The IR absorption spectra in the 4000–400 cm^{-1} region were measured with a Fourier-transform infrared spectrometer (Vertex 80V, Bruker). The spectra were measured at 3 K with 1 cm^{-1} resolution co-adding 200 scans. The matrices were photolyzed by an excimer laser (MSX-250, MPB) operating at 193 nm (~10 mJ cm^{-2} $pulse^{-1}$).

After deposition of an HCl/H_2O/Xe matrix at 40 K, the HCl stretching mode of the HCl···H_2O complex is observed at 2637.7 and 2622.7 cm^{-1} in addition to HCl monomer bands at 2858.0 cm^{-1} (R branch) and 2837.3 cm^{-1} (P branch) [30,37]. Irradiation of HCl/H_2O/Xe matrices at 193 nm leads to the decomposition of the HCl monomer, HCl···H_2O complex, and to some extent H_2O.

Annealing of photolyzed matrices mobilizes H atoms produced by photolysis. In solid Xe, H atoms are known to diffuse at temperatures above 35 K [38]. After annealing of a photolyzed HCl/H_2O/Xe matrix at 40 K, HXeCl monomer (1648.4 cm^{-1}) [1], HXeCl···HCl complex (1661.4, 1671.5, 1675.8, 1685.0, 1754.4 cm^{-1}) [28], HXeCl···H_2O complex (1710.6 and 1730.3 cm^{-1}) [30], HXeOH monomer (1577.6 cm^{-1}) [39], HXeOH···H_2O complex (1680.7 cm^{-1}), and HXeOH···$(H_2O)_2$ complex (1743.8 and

1747.7 cm^{-1}) [40] are observed as indicated in Fig. 4. When the matrix is subsequently annealed at higher temperatures (e.g., at 45 K for 80 min), the HXeCl···H_2O complex band at 1730.3 cm^{-1} disappears almost completely and the band of the HCl···H_2O complex (2634 cm^{-1}) synchronously increases in intensity; see lower trace of Fig. 4. The other band of the HXeCl···H_2O complex (1710.6 cm^{-1}) also decreases in intensity while the decreasing rate is slower than the 1730.3 cm^{-1} band. An increase of the HCl···H_2O complex is not seen after annealing at 45 K of as-deposited HCl/H_2O/Xe matrix, suggesting that the increase of the HCl···H_2O complex seen in a photolyzed matrix is not connected with the mobility of H_2O molecule in a Xe matrix.

The similar results were obtained for HCl/D_2O/Xe matrices. After deposition, the HCl···D_2O complex is observed at 2617.4 and 2625.1 cm^{-1} [30]. Irradiation of HCl/D_2O/Xe matrices at 193 nm leads to the decomposition of the HCl monomer, HCl···D_2O complex, and to some extent D_2O. New absorption appears at 1917 cm^{-1}, which most probably originates from the DCl···HDO complex [41].

After annealing of a photolyzed HCl/D_2O/Xe matrix at 40 K, HXeCl monomer (1648.4 cm^{-1}), HXeCl···HCl complex, and HXeCl···D_2O complex (1712.0 and 1732.3 cm^{-1}) are observed [30]. When the matrix is annealed at higher temperatures (e.g., at 45 K for 80 min), the HXeCl···D_2O complex band at 1732.3 cm^{-1} disappears almost completely and the 2634 cm^{-1} band increases synchronously (Fig. 5). The 2634 cm^{-1} band is presumably due to the HCl···D_2O complex in another matrix site. The other band of the HXeCl···D_2O complex (1712.0 cm^{-1}) also decreases in intensity while the decreasing rate is slower than the 1732.3 cm^{-1} band. Upon annealing at higher temperatures, the formation of DCl···HDO complex, expected at 1917 cm^{-1}, is not seen, as indicated by a yellow rectangle in Fig. 5.

Thermal decomposition of the HXeCl···H_2O complex was studied at five different temperatures from 42 to 46 K. The time variation of the H–Xe stretching absorption intensity at 1730.3 cm^{-1} is plotted in Fig. 6. The decay rates become faster at higher annealing temperatures. The decay curves were fitted by a stretched exponential function of the type $I(t) = I_0 e^{(-\frac{t}{\tau})^{\beta}}$, where I_0 and $I(t)$ are the integrated intensity of the 1730.3 cm^{-1} before annealing and after annealing for a given duration, t, respectively. The stretching exponent, β, accounts for the distribution of different activation energies [42]. The fitted parameters are shown in the lower panel of Fig. 6. The β values decrease from 0.84 at 42 K to 0.65 at 46 K. The similar tendency was found in the thermal decay experiments performed for other matrices. Because the kinetic data are obtained for a single matrix and the range of annealing temperatures is small, the variation might not be due to the effect of matrix morphology [12]. However, we have no clear explanation so far. The time constant, τ, was then converted to the rate constant k (with the dimension $time^{-\beta}$) by a relation of $\ln k = \ln \beta - \beta \ln \tau$. The k values show an Arrhenius behavior. The simple linear regression analysis yielded an activation energy of 15.0 ± 0.6 kJ mol^{-1}.

4. Discussion

According to the theoretical predictions (Table 1), the 2B decomposition barrier height of HXeCl monomer, 97 kJ mol^{-1} at CCSD(T) after considering the effect of Xe environment, becomes smaller, to 62 kJ mol^{-1}, upon complexation with H_2O. On the other hand, the 3B dissociation energy of HXeCl, 78 kJ mol^{-1} in vacuum, increases to 100 kJ mol^{-1} upon complex formation. These changes are consistent with the expectation from spectroscopic observations. The H–Xe stretching frequency blue-shifts from 1648.4 cm^{-1} of HXeCl monomer to 1730.3 cm^{-1} of the HXeCl···H_2O complex, indicating that

complexation stabilize HXeCl with respect to the stretching coordinate and the enhanced ion-pair character, $(HXe)^+Cl^-$, lowers the 2B stabilization barrier. The enhancement of ion-pair character has been seen in the calculated partial atomic charges; the positive charge of the HXe part of the HXeCl monomer is +0.68*e* and upon complexation with H_2O the corresponding charge increases to +0.75*e*, according to the CCSD/def2-TZVPPD level of theory [30].

In experiments, we found that the HXeCl···H_2O complex decomposes at elevated temperatures (≥ 42 K) and produces HCl···H_2O complex as a decomposition product. This result indicates that the thermal decomposition of the HXeCl···H_2O complex in a Xe matrix presumably proceeds through the 2B decomposition channel: i.e., HXeCl···H_2O → Xe + HCl···H_2O. As shown in Figs. 2 and 3, theoretical calculations predicted there are two types of 2B decomposition TS, catalytic and unimolecular TSs, with very similar barrier heights (~62 kJ mol^{-1}). In the catalytic 2B decomposition pathway, H atom in the HXeCl moiety is exchanged with one H atom of water while, in the unimolecular 2B decomposition pathway, the water moiety serves as a spectator. The experiment with HCl/D_2O/Xe mixtures, which selectively produce the HXeCl···D_2O complex, demonstrated that the thermal decomposition product is the HCl···D_2O complex (Fig. 5). Thus, experiments could successfully characterize the thermal decomposition pathway of the HXeCl···D_2O complex to be unimolecular 2B decomposition.

The experimentally determined activation energy for the unimolecular 2B decomposition pathway is 15.0 ± 0.6 kJ mol^{-1}. This value is significantly smaller than the theoretical prediction, ~62 kJ mol^{-1}. This difference might be due to the effect of Xe environment, which cannot be fully modelled by PCM. Indeed, Zhu et al. demonstrated

that to theoretically reproduce the experimental frequency shifts of the H–Xe stretching mode in HXeI monomer in different environments (Ar, Kr, and Xe matrices) sophisticated quantum-chemical approach including the interaction among HXeI and hundreds of surrounding noble-gas atoms is required [15]. To extend such a quantum-chemical approach to the thermal decomposition of HNgY molecules and their complexes is a challenge for future theoretical studies. To date, one such computational study has been reported, in which the molecular dynamics simulations performed by Tsivion and Gerber suggested that HXeCCH in acetylene clusters may be chemically stable up to 150 K [43].

The preferential decomposition through the unimolecular 2B decomposition channel may even indicate the importance of specific interactions between the HXeCl···H_2O complex and surrounding Xe atoms. When we compare the structures of catalytic 2B-TS and unimolecular 2B-TS (Fig. 2), hydrogen atom of the HXeCl moiety in the unimolecular 2B-TS can easily interact with Xe atoms surrounding the complex. However, to prove this hypothesis, an extensive computational work is required and it exceeds the scope of this paper.

Thermal decomposition reactions of the HXeBr···H_2O and HXeI···H_2O complexes have also been investigated by us. Although the interpretations are preliminary, we found decomposition pathways different from that of the HXeCl···H_2O complex. In the case of the HXeBr···H_2O complex, we identified both catalytic and unimolecular 2B decomposition products. In the case of the HXeI···H_2O complex, the HI···H_2O complex was not identified regardless of the decomposition of the HXeI···H_2O complex, indicating that the HXeI···H_2O complex decomposes via the 3B channel; indeed one theoretical calculation suggested a significant reduction of 3B barrier height in HXeI as compared to HXeCl and HXeBr [44]. It is in principle possible that the formation of the

$HCl\cdots H_2O$ (or D_2O) complex can occur following the 3B decomposition channel as $HXeCl\cdots H_2O \rightarrow H + Xe + Cl + H_2O \rightarrow Xe + HCl\cdots H_2O$. However, the observation of the catalytic 2B decomposition product in the case of the $HXeBr\cdots H_2O$ complex and the absence of the $HI\cdots H_2O$ product in the thermal decomposition of the $HXeI\cdots H_2O$ complex support our conclusion that the thermal decomposition of the $HCl\cdots H_2O$ (or D_2O) complex occurs via the 2B decomposition channel. We plan to publish a full paper on these topics in the future.

Finally, we mention the relative stability of HXeCl, HXeBr, and HXeI monomers. In one experiment, we produced HXeCl, HXeBr, and HXeI monomers in a Xe matrix at the same time by photolysis and annealing of an HCl/HBr/HI/Xe matrix. The decay of these monomers was seen upon annealing at temperatures higher than 60 K. The decomposition rate is fastest for HXeCl and slowest for HXeBr, suggesting a trend of thermal stabilities HXeBr > HXeI > HXeCl in a Xe matrix. Actually, explanations for this trend are lucking since both 2B and 3B barriers of HXeCl are predicted to be highest among these three molecules; reported 2B and 3B barriers calculated with the icMRCI+Q method are 144 and 96 kJ mol^{-1} for HXeCl [36], 129 and 75 kJ mol^{-1} for HXeBr [45], and 126 and 35 kJ mol^{-1} for HXeI [44]. These results also indicate that a proper modeling of matrix environments is necessary for predicting thermal stabilities of HNgY molecules.

Declaration of Competing Interest

The authors declare that they have no known competing financial interests or personal relationships that could have appeared to influence the work reported in this paper.

Acknowledgments

M. T. thanks the Academy of Finland for a postdoctoral grant (grant number 1139105). This work is a part of the Project KUMURA of the Academy of Finland (grant number 1277993) and is partially supported by Japan Society for the Promotion of Science (JSPS KAKENHI, grant number JP18K03717). The CSC-IT Center for Science and the Information Initiative Center of Hokkaido University are thanked for computational resources.

References

[1] M. Pettersson, J. Lundell, M. Räsänen, J. Chem. Phys. 102 (1995) 6423.

[2] L. Khriachtchev, M. Räsänen, R.B. Gerber, Acc. Chem. Res. 42 (2009) 183.

[3] W. Grochala, L. Khriachtchev, M. Räsänen, in: L. Khriachtchev (Ed.), Physics and Chemistry at Low Temperatures, 2011, p. 419.

[4] L. Khriachtchev, M. Pettersson, N. Runeberg, J. Lundell, M. Räsänen, Nature 406 (2000) 874.

[5] C. Zhu, M. Räsänen, L. Khriachtchev, J. Chem. Phys. 143 (2015) 244319.

[6] L. Duarte, L. Khriachtchev, Sci. Rep. 7 (2017) 3130.

[7] J. Lundell, L. Khriachtchev, M. Pettersson, M. Räsänen, Low Temp. Phys. 26 (2000) 680.

[8] R.B. Gerber, Annu. Rev. Phys. Chem. 55 (2004) 55.

[9] A. Lignell, L. Khriachtchev, J. Lundell, H. Tanskanen, M. Räsänen, J. Chem. Phys. 125 (2006).

[10] R.B. Gerber, E. Tsivion, L. Khriachtchev, M. Räsänen, Chem. Phys. Lett. 545 (2012) 1.

[11] V.I. Feldman, F.F. Sukhov, Chem. Phys. Lett. 255 (1996) 425.

[12] L. Khriachtchev, H. Tanskanen, M. Pettersson, M. Räsänen, J. Ahokas, H. Kunttu, V. Feldman, J. Chem. Phys. 116 (2002) 5649.

[13] M. Tsuge, S. Berski, R. Stachowski, M. Räsänen, Z. Latajka, L. Khriachtchev, J. Phys. Chem. A 116 (2012) 4510.

[14] M. Tsuge, A. Lignell, M. Räsänen, L. Khriachtchev, J. Chem. Phys. 139 (2013) 204303.

[15] C. Zhu, K. Niimi, T. Taketsugu, M. Tsuge, A. Nakayama, L. Khriachtchev, J.

Chem. Phys. 142 (2015) 054305.

[16] H. Tanskanen, L. Khriachtchev, J. Lundell, M. Räsänen, J. Chem. Phys. 125 (2006).

[17] L. Khriachtchev, K. Isokoski, A. Cohen, M. Räsänen, R.B. Gerber, J. Am. Chem. Soc. 130 (2008) 6114.

[18] E. Tsivion, R.B. Gerber, Chem. Phys. Lett. 482 (2009) 30.

[19] K. Niimi, T. Taketsugu, A. Nakayama, Phys. Chem. Chem. Phys. 17 (2015) 7872.

[20] G.Q. Liu, Y.L. Zhang, Z.X. Wang, Y.Z. Wang, X.X. Zhang, W.X. Zhang, Comput. Theor. Chem. 993 (2012) 118.

[21] J. Kalinowski, R.B. Gerber, M. Räsänen, A. Lignell, L. Khriachtchev, J. Chem. Phys. 140 (2014) 094303.

[22] A. Cohen, M. Tsuge, L. Khriachtchev, M. Räsänen, R.B. Gerber, Chem. Phys. Lett. 594 (2014) 18.

[23] A. Cohen, R.B. Gerber, J. Phys. Chem. A 120 (2016) 3372.

[24] A. Lignell, L. Khriachtchev, J. Mol. Struct. 889 (2008) 1.

[25] A. Corani, A. Domanskaya, L. Khriachtchev, M. Räsänen, A. Lignell, J. Phys. Chem. A 113 (2009) 10687.

[26] A. Lignell, L. Khriachtchev, M. Pettersson, M. Räsänen, J. Chem. Phys. 117 (2002) 961.

[27] A. Lignell, L. Khriachtchev, M. Pettersson, M. Räsänen, J. Chem. Phys. 118 (2003) 11120.

[28] A. Lignell, J. Lundell, L. Khriachtchev, M. Räsänen, J. Phys. Chem. A 112 (2008) 5486.

[29] M. Tsuge, S. Berski, M. Räsänen, Z. Latajka, L. Khriachtchev, J. Chem. Phys. 138

(2013) 104314.

[30] M. Tsuge, S. Berski, M. Räsänen, Z. Latajka, L. Khriachtchev, J. Chem. Phys. 140 (2014) 044323.

[31] K.L. Schuchardt, B.T. Didier, T. Elsethagen, L. Sun, V. Gurumoorthi, J. Chase, J. Li, T.L. Windus, J. Chem. Inf. Model. 47 (2007) 1045.

[32] S.F. Boys, F. Bernardi, Mol. Phys. 19 (1970) 553.

[33] J. Tomasi, B. Mennucci, R. Cammi, Chem. Rev. 105 (2005) 2999.

[34] H. Li, D. Xie, H. Guo, J. Chem. Phys. 120 (2004) 4273.

[35] G.M. Chaban, J. Lundell, R.B. Gerber, Chem. Phys. Lett. 364 (2002) 628.

[36] Z.G. Huang, D.Q. Xie, H. Zhu, Sci. China, Ser. B 50 (2007) 7.

[37] A.J. Barnes, H.E. Hallam, G.F. Scrimsha, Trans. Faraday Soc. 65 (1969) 3159.

[38] L. Khriachtchev, H. Tanskanen, M. Pettersson, M. Räsänen, V. Feldman, F. Sukhov, A. Orlov, A.F. Shestakov, J. Chem. Phys. 116 (2002) 5708.

[39] M. Pettersson, L. Khriachtchev, J. Lundell, M. Räsänen, J. Am. Chem. Soc. 121 (1999) 11904.

[40] A.V. Nemukhin, B.L. Grigorenko, L. Khriachtchev, H. Tanskanen, M. Pettersson, M. Räsänen, J. Am. Chem. Soc. 124 (2002) 10706.

[41] A. Engdahl, B. Nelander, J. Chem. Phys. 84 (1986) 1981.

[42] A. Plonka, Time-Dependent Reactivity of Species in Condensed Media, Springer-Verlag, Berlin, 1986.

[43] E. Tsivion, R.B. Gerber, Phys. Chem. Chem. Phys. 13 (2011) 19601.

[44] Z.G. Huang, E.C. Yang, D.Q. Xie, J. Mol. Struct.: THEOCHEM 867 (2008) 95.

[45] Z.G. Huang, E.C. Yang, D.Q. Xie, Chin. Chem. Lett. 19 (2008) 627.

Table 1

Barrier heights of 2B decomposition and dissociation energies of 3B decomposition for HXeCl monomer and the HXeCl···H_2O complex calculated with the MP2(full) and CCSD(T) methods using the def2-TZVPPD basis set.[a]

	MP2(full)		CCSD(T)		literature[b]
	vacuum	PCM(Xe)	vacuum	PCM(Xe)[c]	
HXeCl monomer					
2B	124	92	131	97	144
3B			78[d]		96[e]
HXeCl···H_2O complex					
Catalytic 2B	74	55	83	62	
Unimolecular 2B	74	55	83	62	
3B			100[f]		

[a]Energies (in kJ mol^{-1}) are corrected for zero-point vibrational energy and BSSE.

[b]icMRCI + Q method.[36]

[c]Because PCM is not available for the CCSD(T) method, the effect of Xe is taken into account by using the ratio calculated with the MP2(full) method (see text).

[d]3B dissociation energy calculated as the energy difference between ″H + Xe + Cl″ asymptote and the equilibrium structure of HXeCl monomer.

[e]3B dissociation barrier.

[f]3B dissociation energy calculated as the energy difference between ″H + Xe + Cl + H_2O″ asymptote and the equilibrium structure of the HXeCl···H_2O complex.

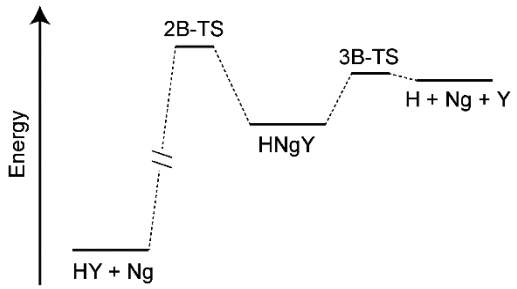

Fig. 1. The general energy diagram of noble-gas hydride, HNgY. 2B-TS: two-body decomposition transition state. 3B-TS: three-body decomposition transition state. (single column)

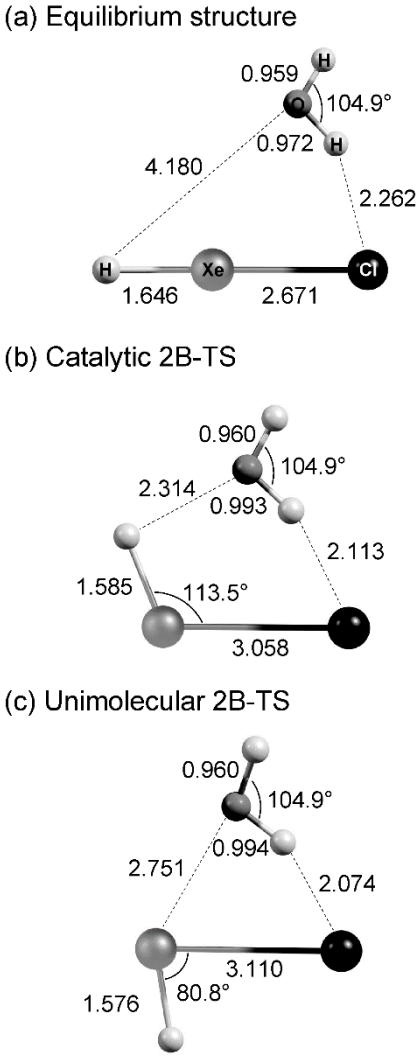

Fig. 2. Structures of the HXeCl···H_2O complex at (a) equilibrium, (b) catalytic two-body decomposition transition state (2B-TS), and (c) unimolecular 2B-TS optimized with the CCSD(T)/def2-TZVPPD method. Important structural parameters are indicated; bond lengths are in Å.

(single column)

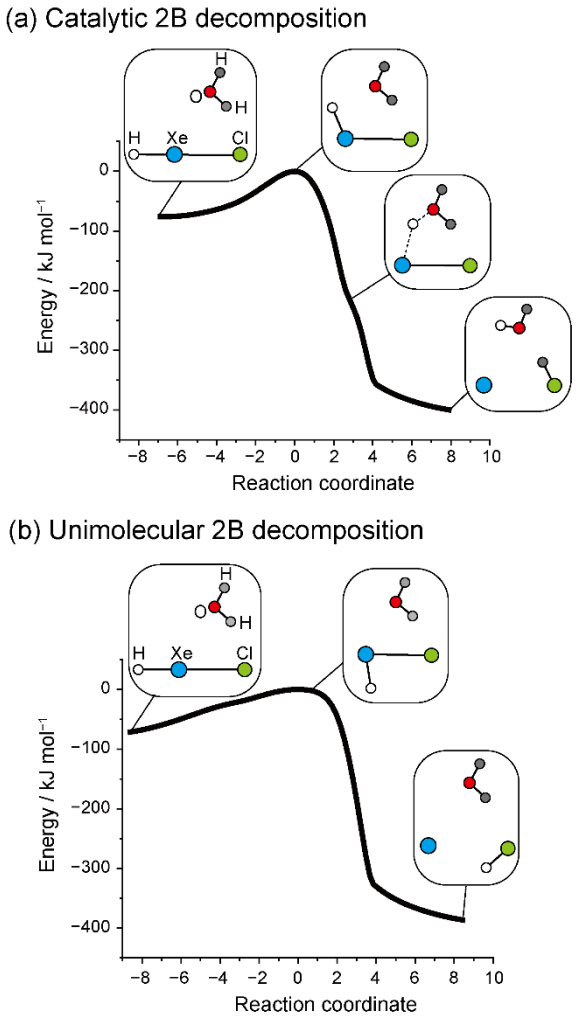

Fig. 3. Reaction paths along the intrinsic reaction coordinate for (a) catalytic 2B decomposition and (b) unimolecular 2B decomposition. Calculations were performed with the MP2/def2-TZVPPD method. Hydrogen atoms in the HXeCl and H_2O moieties are shown in different colors (white and dark gray, respectively) so that the hydrogen exchange in the catalytic decomposition process is easily recognized.

(single column, color online)

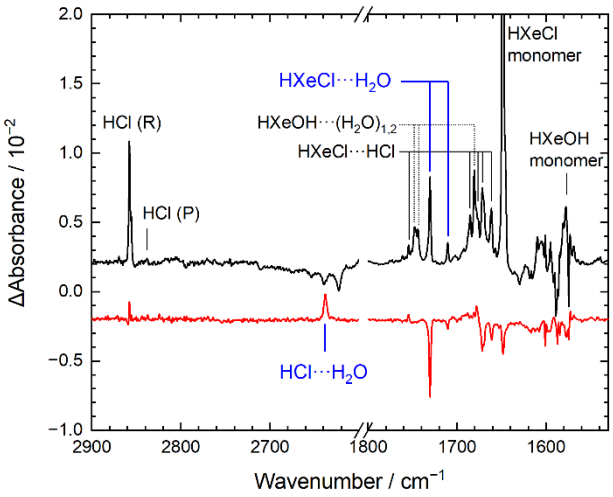

Fig. 4. Infrared difference spectra showing the results of (upper) annealing at 40 K of the photolyzed $HCl/H_2O/Xe$ matrix and (lower) subsequent annealing at 45 K. Prior to these experimental steps, the $HCl/H_2O/Xe$ matrix deposited at 40 K was photolyzed by 193 nm light. Spectra were measured at 3 K.

(single column, color online)

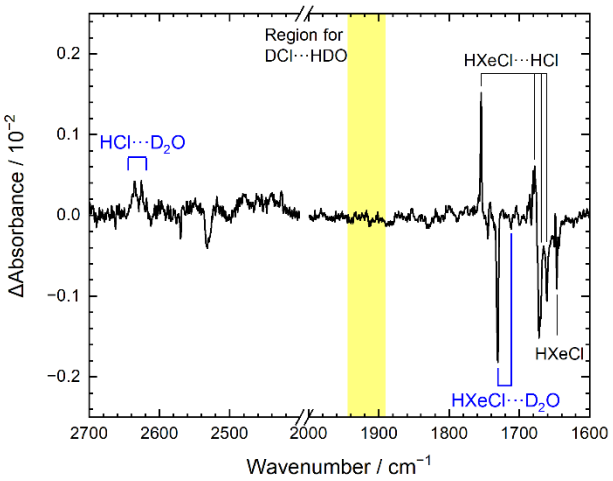

Fig. 5. Infrared difference spectrum of an HCl/D_2O/Xe matrix showing the result of annealing at 45 K for 80 min. Before this experimental step, the HXeCl···D_2O complex was produced by photolysis at 193 nm followed by annealing at 40 K for 80 min. The spectra were measured at 3 K. The absence of the DCl···HDO complex is indicated with a yellow rectangle.

(single column, color online)

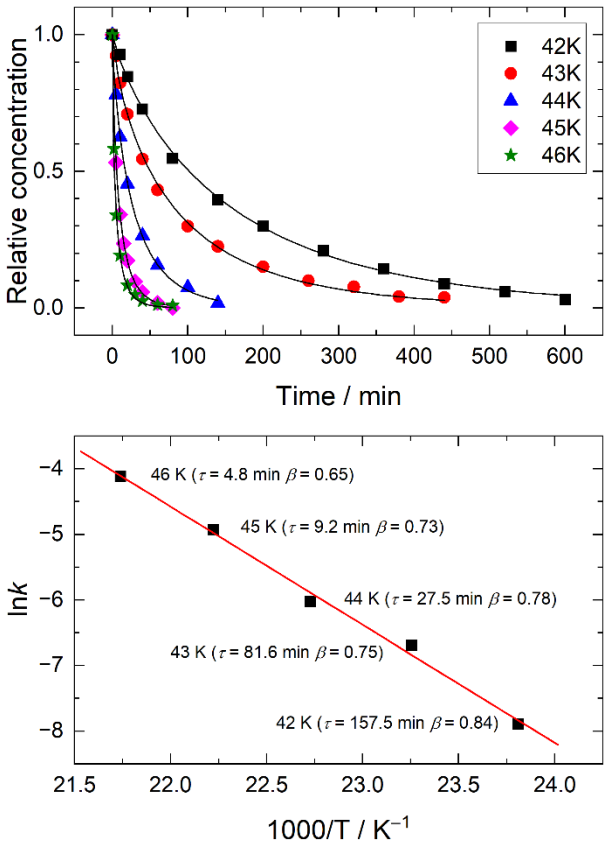

Fig. 6. Upper: Thermal decomposition of the HXeCl···HCl complex at temperatures 42–46 K. The experiment was performed for a single matrix sample by varying annealing temperature from low to high. Solid lines represent the results of least-square fits with the stretched exponential function. Lower: Arrhenius plot of the decomposition. Parameters (decay time constant, τ, and stretching exponent, β) determined for each temperature are indicated. The solid line represents the simple linear regression.

(single column, color online)